JOURNAL OF CATALYSIS 125, 227–242 (1990)

Cooperative Behavior of Two Kinds of Reaction Sites and Reaction Mechanisms for Deuteration of Acrolein on SMSI-Pt/Nb_2O_5 Catalyst

HIDEAKI YOSHITAKE AND YASUHIRO IWASAWA[1]

Department of Chemistry, Faculty of Science, University of Tokyo, Hongo, Bunkyo-ku, Tokyo 113, Japan

Received December 4, 1989; revised February 23, 1990

The mechanism of the deuteration of acrolein in the formation of propanal and allyl alcohol over normal (LTR-) and SMSI-Pt/Nb_2O_5 was investigated in order to clarify the structure and chemical environment of the reaction sites and their microscopic behavior in the working state, in relation to general promoter/poisoning phenomena. The reaction on the LTR catalyst follows a conventional associative mechanism involving η^2(C–C) or η^2(C–O) species. In contrast, as is seen from the reaction rates as a function of the reduction time of the catalyst, together with the isotope distributions in the products, both propanal and allyl alcohol on the SMSI catalyst are formed through η^4(C–C–C–O)-intermediates on the peripheral sites of migrated NbO_x islands, where deuterium atoms are supplied from bare metal sites on which deuterium is dissociatively adsorbed. A large isotope effect (one-tenth) on the rate of allyl alcohol formation when d_0-acrolein was replaced by d_4-acrolein was observed with the SMSI catalyst, suggesting a hydrogen-induced γ-C–H breaking mechanism. The kinetic parameters were compared with those for deuteration of 3,3,3-trifluoropropene, which has a CF_3 group with a Hammett's parameter similar to that of the CHO group of acrolein, in order to examine the contribution of the conjugation of C=C and C=O ion acrolein to the adsorption and to the reaction taking place on the SMSI surface. The reaction mechanisms for the LTR and SMSI catalysts are described and discussed in relation to electronic and geometric factors for the origin of cooperative catalysis. The differences in catalytic behavior among the SMSI metal (Pt, Ir, and Rh) catalysts are also discussed in terms of their electronic structures.

INTRODUCTION

Catalytic properties as well as structural features of supported metal catalysts in the SMSI state have been studied extensively (*1–6*). SMSI catalysts can be regarded as a model of additive/promoter effects because their catalysis includes both poisoning and promoting phenomena, which may be derived from the migration of suboxides (*7–10*) accompanied by perturbation of the metal electronic state (*11, 12*). Suppression of the adsorption capacity by SMSI is believed to result in a decrease in the rates of almost-catalytic reactions, but the extent of suppression is not constant even among the same kinds of hydrogenations (*1*). In contrast, the methanation reaction has been reported to be enhanced in the SMSI state (*13–28*), which has often been attributed to the relatively small suppression of H_2 chemisorption and the activation of CO adsorbed at the metal–support (or suboxide) interface. Investigation of the catalytic reaction mechanism involving the behavior of adsorbed species rather than static profiles such as adsorption, may be of great importance to understanding the origin of supported metal catalysis and the role of promoters. Kinetic studies on the hydrogenation of benzene (*29, 38*), acetone (*31*), and crotonaldehyde (*32*) that showed that SMSI changes not only the catalytic activity but also the reaction path have been reported. We have studied the deuteration mechanisms of ethene (*33*) and acrolein (*34*) on Rh/Nb_2O_5 and Ir/Nb_2O_5 by kinetics and isotope tracing methods in order to explain the microscopic behavior of reaction sites, their chemical environments, and the

[1] To whom correspondence should be addressed.

0021-9517/90 $3.00

factors involved in the activation of molecules in the SMSI state, which could be elucidated only under dynamic reaction conditions. Acrolein is the simplest α,β-unsaturated carbonyl compound that has a polarized conjugate system. The previous report showed that the mechanism of acrolein deuteration and the distribution of deuterium can be sensitive probes of the nature and change of reaction sites on metal surfaces (*34, 36*). In the present report we chose the same substance as a test molecule for investigating the synergistic behavior of active sites and the reaction mechanism of deuteration on Pt/Nb_2O_5 in normal and SMSI states. In addition, the deuteration of 3,3,3 trifluoropropene (CH_2=$CHCF_3$) was performed in order to compare the acrolein C=C double bond and the nonconjugated C=C double bond; the CF_3 group is almost the same as the CHO group in electron-withdrawing character.

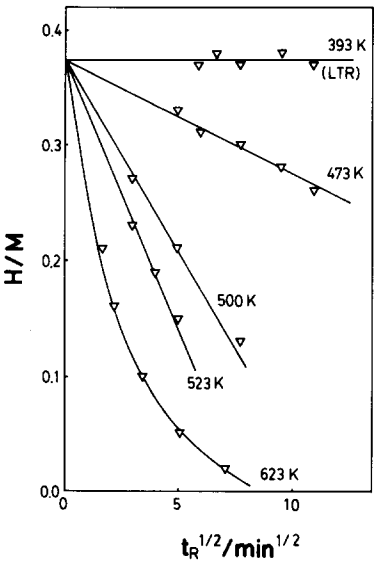

FIG. 1. H/*M* values versus catalyst reduction times at several temperatures.

METHODS

Nb_2O_5-supported platinum catalyst was prepared by a conventional impregnation method with an aqueous solution of $H_2PtCl_6 \cdot 6H_2O$ (Soekawa Chemical), dried for 3 h at 393 K, and calcined for 2 h at 773 K in air. Commercially available Nb_2O_5 (Soekawa Chemical; BET surface area 5 $m^2 \cdot g^{-1}$) was used as support. The metal loading was 2.5 wt%. The catalyst thus obtained was placed in a closed circulating system (dead volume 130 cm^3). It was then treated with oxygen for 1 h at 673 K, followed by evacuation for 30 min, and reduced for 1 h at 393 K (LTR) or 773 K (HTR), followed by evacuation for 30 min before each catalytic reaction. The particle size of the platinum metal was determined to be 3.9 nm by transmission electron microscopy.

Acrolein (purchased from Tokyo Kasei) and 3,3,3-trifluoropropene (99.5%, Japan Halon Co.) were further purified by freeze–thaw cycles. Hydrogen and deuterium gases of research grade were purified through a 5-Å molecular sieve trap at 77 K. Typical reaction gas pressure was 1.3 kPa for acrolein and 5.3 kPa for deuterium (or a mixture of deuterium and hydrogen). The deuterated products of the reactions were analyzed by gas chromatography with a TCD detector or by a mass spectrometer (ULVAC MSQ-150A operating with 70-eV electrons) after separation on the column; propanal, allyl alcohol (prop-2-en-1-ol), 1-propanol, and acrolein were separated on a 2-m PEG-1500 column at 333 K, and 3,3,3-trifluoropropene and 1,1,1-trifluoropropane on a 2-m VZ-10 column at 343 K. The usual corrections in the mass spectroscopic analysis were made for natural isotopes and for the first C–H and C–D fragmentation, which corresponds to the fragmentation of aldehydic hydrogen. The other corrections were small enough to be neglected.

RESULTS

The amounts of hydrogen adsorbed on Pt/Nb_2O_5 reduced at various temperatures are illustrated in Fig. 1. Each measurement was conducted on the same sample after oxidation (673 K)–reduction treatments. The reversibility of the H/*M* value in oxidation–reduction treatments was confirmed. Plots of

TABLE 1

Initial Rates and Activation Energies for the Deuteration of CH_2=CHCH=O and CH_2=$CHCF_3$ and for the H_2–D_2 Exchange Reaction

Reaction	Product[a]	r_{LTR}[b]	E_A^{LTR}	r_{HTR}[b]	E_A^{HTR}	r_{HTR}/r_{LTR}
D_2 + CH_2=CHCHO	PA	0.737	5	0.041	46	5.6×10^{-2}
(373 K)	AA	0.224	5	0.094	44	4.2×10^{-1}
	PO	0.318	7	0.000		0.0
D_2 + CD_2=CDCDO	PA	0.740		0.040		5.4×10^{-2}
(373 K)	AA	0.201		0.009		4.5×10^{-2}
	PO	0.288		0.000		—
H_2 + D_2 + CH_2=CHCHO	HD	1.32	5	0.406	19	3.1×10^{-1}
(373 K)						
D_2 + CH_2=$CHCF_3$	$EtCF_3$	1.18	9	2.1×10^{-4}	9	1.7×10^{-4}
(273 K)						
H_2 + D_2 + CH_2=$CHCF_3$	HD	1.20	8	0.376	17	3.1×10^{-1}
(273 K)						
		Pt/SiO_2				
D_2 + CH_2=CHCHO	PA	0.132	6			
(373 K)	AA	0.00				
	PO	0.00				

[a] PA, AA, and PO represent propanal, allyl alcohol, and propanol, respectively. Other products, such as ethane and carbon monoxide, are less than 1% under our conditions.

[b] r_{LTR} and r_{HTR} represent the initial rates (min^{-1}, normalized by $H/M = 0.375$) for LTR and HTR catalysts respectively. E_A is activation energy ($kJ \cdot mol^{-1}$). Reaction temperature is between 333 and 393 K. CH_2=CHCHO, CD_2=CDCDO, CH_2=$CHCF_3$: 1.3 kPa; total hydrogen (H_2, D_2, or H_2 + D_2): 5.3 kPa.

the H/M value vs the square root of the reduction time ($t_R^{1/2}$) were extrapolated to the same value, i.e., $H/M = 0.375$ at $t_R = 0$, which agrees with H/M for the LTR catalyst, $(H/M)_{LTR}$. $(H/M)_{LTR}$ did not change with $t_R^{1/2}$. H/M for the HTR (reduced at 773 K) catalyst, $(H/M)_{HTR}$, was below the detection limit (<0.01) of our experiment. H/M curves were observed to be proportional to the square root of t_R (7), consistent with the experiment of Resasco and Haller. No significant sintering of Pt particles during HTR treatment was observed by TEM.

The initial rates and activation energies for the deuteration of acrolein and 3,3,3-trifluoropropene are listed in Table 1. The selectivities to propanal, allyl alcohol, and propanol in d_0-acrolein deuteration on the LTR catalyst are 58, 17, and 25%, respectively, while those on the HTR catalyst are 30, 70, and 0%, as shown in Table 1. On Pt/SiO_2 only propanal was formed under the same conditions. Hydrogenolysis is negligible and no acceleration of rates which is often found in CO–H_2 reactions, was observed. A significant isotope effect in acrolein–hydrogen for allyl alcohol formation was observed with the HTR catalyst, on which the rate for D_2/CH_2=CHCHO was 10 times higher than that for D_2/CD_2=CDCDO, while negligible isotope effects were observed for propanal formation on both the LTR and the HTR catalysts and for allyl alcohol formation on the LTR catalyst.

The activities and the activation energies for the H_2–D_2 exchange reaction on the LTR catalyst under acrolein deuteration conditions are the same as those for the deuteration of acrolein. On the other hand, they are different from those for the HTR catalyst.

A comparison of the C=C hydrogenation rate between acrolein and 3,3,3-trifluoropropene shows the influence of the conjugation on this reaction. On the LTR catalyst the rate of 1,1,1-trifluoropropane formation is higher than that of propanal formation by a factor of 1.6, but lower by a factor of 5.1×10^{-3} on the HTR catalyst. The H_2–D_2 exchange reaction under 3,3,3-trifluoropropene deuteration showed the same feature as that under acrolein deuteration.

There is a possibility of a secondary reaction of allyl alcohol under the reaction conditions; allyl alcohol is the most unstable product among the three (allyl alcohol (AA): $\Delta H_f = -124.2$ kJ · mol^{-1}; propanal (PA): $\Delta H_f = -187.4$ kJ · mol^{-1}; propanol (PO): $\Delta H_f = -254.8$ kJ · mol^{-1}). Deuteration of a mixture of acrolein (AC) and allyl alcohol was carried out at $P_{AA} + P_{AC} = 1.3$ kPa and $P_{H_2} = 5.3$ kPa, and the rate was normalized by r_0 (rate at $P_{AA} = 0$ kPa), as shown in Fig. 2. Allyl alcohol is converted to propanol mainly by further hydrogenation and suppresses acrolein consumption on the LTR catalyst, while it is converted to propanal mainly through isomerization on the HTR catalyst. This behavior is consistent with the time profile for the product formation in the D_2/CH_2=CHCHO reaction on both catalysts; allyl alcohol formation saturates on both catalysts, while neither propanol nor propanal achieves saturation in the formation on the LTR or the HTR catalyst.

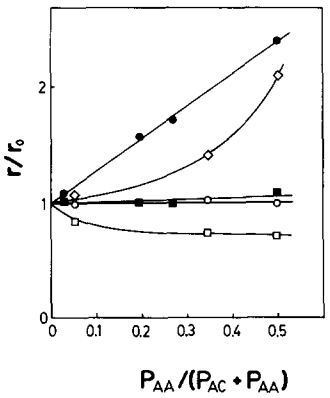

FIG. 2. Variation in the initial rates (r) with the amount of allyl alcohol added; r_0 is the initial rate without allyl alcohol added. LTR catalyst: (○) propanal, (◇) propanol, (□) acrolein; HTR catalyst: (●) propanal, (■) acrolein.

TABLE 2

Percentage Distribution of Deuterated Acrolein in the Initial Stage of D_2–Acrolein Reaction at 373 K

	Product	Catalyst	
		LTR	HTR
d_0	CH_2=CHCHO	90	91
d_1	CHD=CHCHO	3	8
	CH_2=CDCHO	0	1
	CH_2=CHCDO	7	0
	$100\,\Sigma id_i/4\Sigma d_i$	2.5	2.3

Note. Values at 8% conversion of deuteration. CH_2=CHCHO, 1.3 kPa; D_2, 5.3 kPa.

Isotope distributions of the products in the D_2/CH_2=CHCHO reaction are listed in Tables 2–4. Exchange of hydrogen between AC and D_2 occurs at aldehydic hydrogens (7%) and terminal hydrogens (3%) on the LTR catalyst, while it was observed mainly at the latter position on the HTR catalyst, as shown in Table 2. The exchange yields are not different for the two catalysts.

Deuterium was observed on β- and γ-carbon atoms in propanal for both catalysts, as shown in Table 3. The ratio of γ-d_1 to β-d_1 is 14:9 for LTR and 31:4 for HTR; i.e., terminal carbon is preferable in deuterium addition for both catalysts but the selectivity is much greater with the HTR catalyst. The amount of deuterium incorporated in the produced propanal ($\Sigma id_i/n\Sigma d_i$, where n is the number of intrahydrogens related to the reaction) is much less for the HTR than for the LTR catalyst, which reflects the surface D/H ratio under reaction conditions.

Deuterium addition for allyl alcohol formation on the LTR catalyst occurs at the C=O double bond, as shown in Table 4. In contrast, the main site of deuterium incorporation for the HTR catalyst is the terminal

TABLE 3

Percentage Distribution of Deuterated Propanal in the Initial Stage of D_2–Acrolein Reaction at 373 K

	Product	Catalyst	
		LTR	HTR
d_0	$CH_3CH_2CH{=}O$	0	13
d_1	$CH_2DCH_2CH{=}O$	14	31
	$CH_3CHDCH{=}O$	9	4
d_2	$CHD_2CH_2CH{=}O$	23	29
	$CH_2DCHDCH{=}O$	16	20
	$CH_3CD_2CH{=}O$	11	3
d_3	$CD_3CH_2CH{=}O$	10	0
	$CHD_2CHDCH{=}O$	7	0
	$CH_2DCD_2CH{=}O$	5	0
d_4	$CD_3CHDCD{=}O$	4	0
	$CHD_2CD_2CH{=}O$	1	0
	$100\,\Sigma id_i/6\Sigma d_i$	35(42)	23(28)

Note. Values in parentheses are $100\,\Sigma id_i/5\Sigma d_i$. $\Sigma id_i/5\Sigma d_i$ is a reasonable parameter for the LTR catalyst because the hydrogen in –CH=O is not involved with the hydrogenation of C=C; consequently, it is comparable with Table 5 (see text). The values are extrapolated to 0% conversion. $CH_2{=}CHCHO$, 1.3 kPa; D_2, 5.3 kPa.

carbon. The $\Sigma id_i/n\Sigma d_i$ value is lower with the HTR than with the LTR catalyst, similar to the case of propanal.

The significant difference between the two catalysts in the deuterium distribution

TABLE 4

Percentage Distribution of Deuterated Allyl Alcohol in the Initial Stage of D_2–Acrolein Reaction at 373 K

	Product	LTR	HTR
d_0	$CH_2{=}CHCH_2OH$	16	12
d_1	$CH_2{=}CHCH_2OD$	4	4
	$CH_2{=}CHCHDOH$	29	2
	$CHD{=}CHCH_2OH$	0	62
d_2	$CH_2{=}CHCHDOD$	41	0
	$CHD{=}CHCH_2OD$	0	3
	$CD_2{=}CHCH_2OH$	0	17
d_3	$CH_2{=}CHCD_2OD$	10	0
	$100\,\Sigma id_i/6\Sigma d_i$	24(48)	18(36)

Note. Values in parentheses are $100\,\Sigma id_i/3\Sigma d_i$. The values are extrapolated to 0% conversion. $CH_2{=}CHCHO$, 1.3 kPa; D_2, 5.3 kPa.

TABLE 5

Percentage Distribution of Deuterated 1,1,1-Trifluoropropane and 3,3,3-Trifloropropene in the Initial State of D_2–$CH_2{=}CHCF_3$ Reaction at 310 K

	Product	LTR	HTR
d_0	$CH_3CH_2CF_3$	4	21
d_1	$CH_2DCH_2CF_3$	19	33
d_2	$CHD_2CH_2CF_3$	28	38
	$CH_2DCHDCF_3$	9	8
d_3	$CD_3CH_2CF_3$	15	0
	CHD_2CHDCF_3	8	0
d_4	CD_3CHDCF_3	8	0
	$CHD_2CD_2CF_3$	6	0
d_5	$CD_3CD_2CF_3$	3	0
	$\Sigma id_i/5\Sigma d_i$	47	25
d_0	$CH_2{=}CH_2CF_3$	98	98
d_1	$CHD{=}CH_2CF_3$	2	2

Note. The values are extrapolated to 0% conversion for deuterated products and 8% conversion for exchanged products. $CH_2{=}CHCHO$, 1.3 kPa; D_2, 5.3 kPa.

in 1,1,1-trifluoropropane formed in the D_2/3,3,3-trifluoropropene reaction is the amount of deuterium incorporated (Table 5); it is much lower with the HTR catalyst than with the LTR catalyst. The profile of $\Sigma id_i/n\Sigma d_i$ is similar to that of propanal.

Deuteration rates for each product were measured in the course of generating the SMSI state at different reduction temperatures as a function of reduction time (Fig. 3). Each measurement was taken on the same sample after oxidation–reduction treatment, and the data show good reproducibility. All rates are normalized by $H/M = 0.375$. At 393 K reduction, the rates are constant against the reduction time t_R of the catalyst. On the other hand, at 473 K reduction, propanol shows a maximum at ca. $t_R = 40$ min. The rates of allyl alcohol and propanal formation on the catalyst prereduced at 623 K show a maximum at ca. $t_R = 20$ min, while they are almost constant against t_R for the catalyst reduced at 773 K. The behaviors of the rates for allyl alcohol and propanal formations (Fig. 3) are the

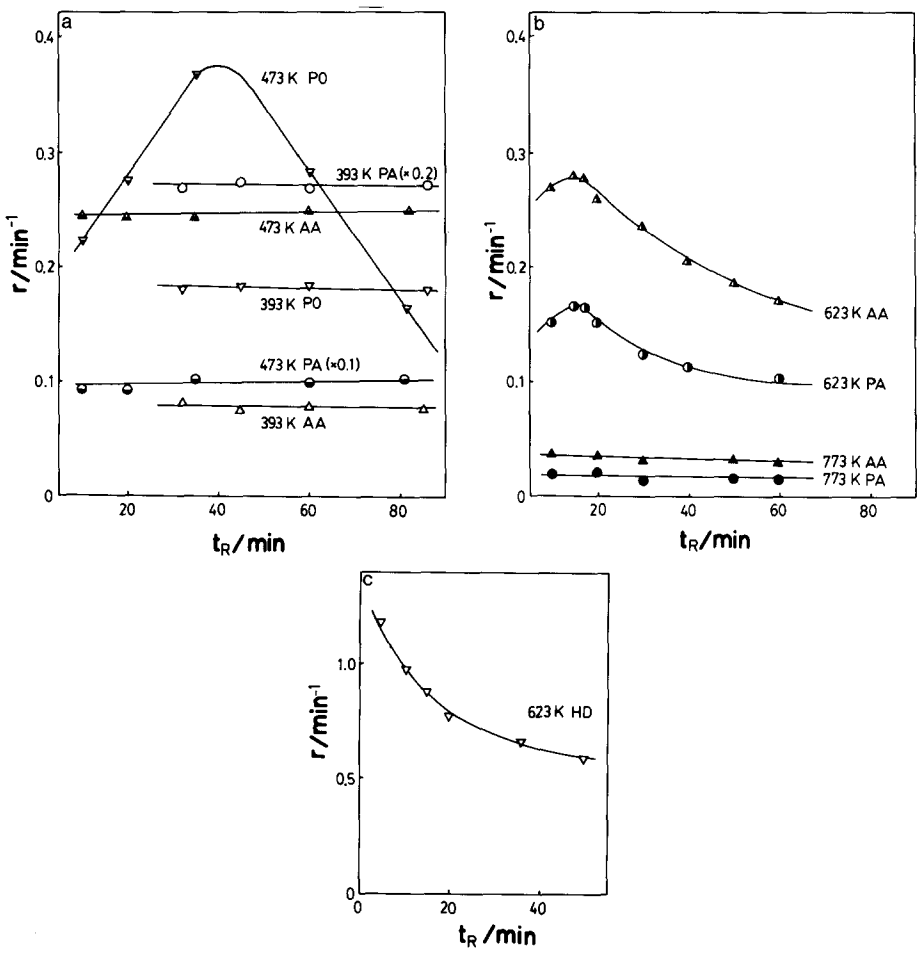

FIG. 3 (a) Rates (turnover frequencies: TOF) of product formation at 373 K versus catalyst reduction times (t_R) at 393 and 473 K; acrolein, 1.3 kPa; D_2, 5.3 kPa. TOF was calculated by using $H/M = 0.375$. (○, ◒) Propanal; (△, ▲) allyl alcohol; (▽, ▼) propanol. (b) Rates (TOF) of product formation at 373 K versus catalyst reduction times (t_R) at 623 and 773 K; acrolein, 1.3 kPa; D_2, 5.3 kPa. TOF was calculated using $H/M = 0.375$. (◑, ●) Propanal; (◭, ▲) allyl alcohol. (c) Rates (TOF) of HD formation at 373 K versus catalyst reduction times (t_R) at 623 K; acrolein, 1.3 kPa; H_2, 2.6 kPa; D_2, 2.6 kPa. TOF was calculated by using $H/M = 0.375$.

same except in absolute value. Figures 3a and 3b also demonstrate that the choice of reduction temperature for LTR (T_R = 393 K) and HTR (T_R = 773 K) was adequate. The H_2–D_2 exchange in the $H_2 + D_2/CH_2$ = CHCHO reaction was also monitored against t_R in the reduction at 623 K (Fig. 3c). The rate decreased monotonously, unlike that of propanal and allyl alcohol formation.

To explore the origin of the isotope effect in deuteration of CH_2=CHCHO and CD_2=CDCDO, two kinds of transient isotope-tracing experiments were performed, as shown in Figs. 4 and 5 and Table 6. CH_2=CHCHO was introduced during the D_2/CD_2=CDCDO reaction (Fig. 4). The profile of allyl alcohol formation is characterized by the rate enhancement with the induction period after the emergence of CH_2=CHCHO in the gas phase. Propanal formation also increased slightly after CH_2=CHCHO addition. In Fig. 5, H_2 was introduced during the

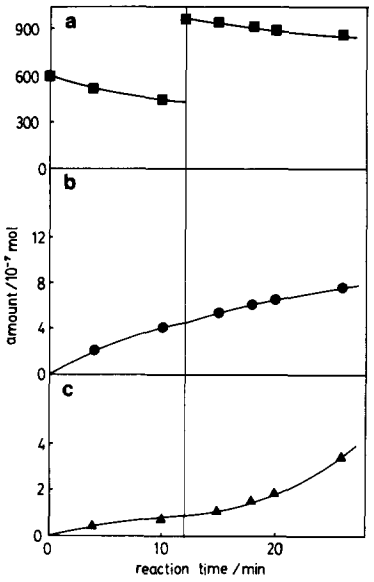

FIG. 4. Transient behavior of (a) acrolein, (b) propanal, and (c) allyl alcohol produced by d_0-acrolein addition during d_4-acrolein deuteration on the SMSI-Pt/Nb_2O_5 catalyst at 373 K; d_4-acrolein, 1.3 kPa; D_2, 5.3 kPa; d_0-acrolein, 1.3 kPa. d_0-Acrolein was added at t = 12 min.

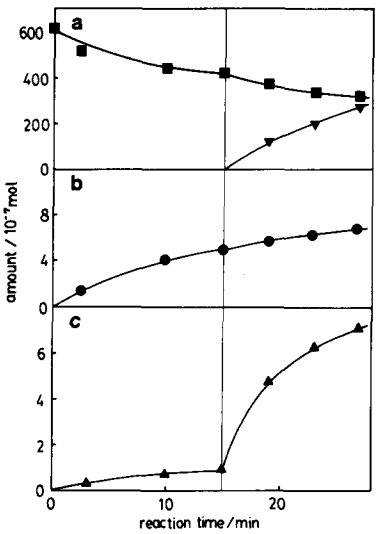

FIG. 5. Transient behavior of each product produced by hydrogen addition during d_4-acrolein deuteration on the SMSI catalyst at 373 K; d_4-acrolein, 1.3 kPa; D_2, 5.3 kPa; H_2, 5.3 kPa. H_2 was added at t = 15 min. (a) ■, Acrolein; ▼, HD. (b) Propanal. (c) Allyl alcohol.

TABLE 6

Isotope Distribution in Allyl Alcohol Formed 10 min after H_2 Introduction to the D_2/CD_2=CDCDO System on HTR Catalyst

		Exper.	Calc.[a]
d_6	CD_2=$CDCD_2OD$	19	16
d_5	CHD=$CDCD_2OD$	10	13
	CD_2=$CDCD_2OH$	37	39
d_4	CHD=$CDCD_2OH$	35	32

Note. CD_2=CDCDO, 1.3 kPa; D_2, 5.3 kPa.
[a] See text.

D_2/CD_2=CDCDO reaction. HD formation is a hundred times as rapid as the formation of propanal and allyl alcohol. The rate of allyl alcohol formation is remarkably enhanced with no induction period, while the enhancement for propanal was enhanced only slightly. The isotope distributions in allyl alcohol in the initial stage of transient reaction are listed in Table 6.

Table 7 shows the result of another kind of transient isotope tracing study which provides information about active sites for allyl alcohol isomerization under D_2/CD_2=CDCDO reaction conditions. d_0-Allyl alcohol was introduced into the D_2/CD_2=CDCDO system. All d_0–d_6-propanals were produced in the initial stage of the isomerization of allyl alcohol.

DISCUSSION

(*i*) *Hydrogen Adsorption*

It is widely believed that the suppression of hydrogen adsorption by high-temperature

TABLE 7

Isotope Distribution in Propanal Formed by d_0-Allyl Alcohol Addition during the Course of d_4-Acrolein Deuteration on HTR Catalyst

	d_0	d_1	d_2	d_3	d_4	d_5	d_6
Relative amount (%)	10	13	36	5	6	8	22

Note. CD_2=CDCDO, CH_2=$CHCH_2OH$: 1.3 kPa; D_2: 5.3 kPa.

reduction of TiO_2- or Nb_2O_5-supported metal catalysts is due to the migration of partially reduced support oxide onto the metal surfaces (*1, 3, 4, 6–10*). The H/*M* value is proportional to the square root of t_R in the reduction temperature range $T_R < 623$ K, as shown in Fig. 1. It is likely that the migration of the suboxides onto metal surfaces is subjected to thermal diffusion processes, consistent with Refs. (*7*) and (*35*). The activation energy of the process on Pt/Nb_2O_5 was determined to be 94 kJ · mol^{-1}. On the other hand, H/*M* for reduction temperatures $T_R \geq 623$ K was not the case. This may be due to the repulsion of NbO_x islands and/or to the change in growth mode, e.g., from two- to three-dimensional.

(*ii*) *Kinetic Properties*

The suppression of catalytic activity by SMSI has been reported to depend on the type of reaction and metal (*1, 29*). In our previous report (*33, 34*), the deuteration of ethene or acrolein over Rh/Nb_2O_5 or Ir/Nb_2O_5 catalysts was suppressed by a factor of 10–100 by HTR. In this context, the careful choice of a standard of reaction is important for comparing activities and exploring the origin of catalysis.

Acrolein, with C=C and C=O double bonds, is a probe molecule used to investigate the dynamic behavior of adspecies and reaction sites. In most cases, hydrogenation occurs preferentially on the C=C double bond. The carbonyl bond seems to have no interaction with the metal surface. In contrast, the Nb_2O_5-supported Pt catalyst produces a significant amount of C=O hydrogenated molecules. In particular, the SMSI-Pt/Nb_2O_5 catalyst showed selective formation of allyl alcohol, as shown in Table 1. Recently, Vannice *et al.* reported that hydrogenation of crotonaldehyde (CH_3CH=-CHCHO) caused the formation of the corresponding unsaturated alcohol on Pt/TiO_2, while no alcohol was formed on Pt/SiO_2 (*32*). Their results are similar to ours, past (*34*) and present. A drastic improvement in selectivity often includes a mechanistic change.

The activation energy (5 kJ · mol^{-1}) for H_2–D_2 exchange coincides with those for propanal and allyl alcohol formation on the LTR-Pt/Nb_2O_5 catalyst, as shown in Table 1. The initial rates of propanal and allyl alcohol formation were nearly proportional to the hydrogen pressure. These similar kinetic parameters suggest that the reaction environments for the formation of both products on the LTR catalyst are similar, that both reactions involve a common rate-determining step which is also common to that for H_2–D_2 exchange in the presence of acrolein, and hence that the rate-determining step is the dissociative adsorption of hydrogen, which is similar to the result observed with Ir/Nb_2O_5 (*34*). On the SMSI catalyst, however, the rate of HD formation is significantly higher than that for both deuterated products, and the activation energy is much lower for HD formation (19 kJ · mol^{-1}) than that for both products (46 and 45 kJ · mol^{-1}). The rate-determining step is thought to shift to the other step. The isotope effect between D_2/CD_2=CHCHO and D_2/CD_2=CDCDO reactions observed in Table 1 suggests that the rate-determining step for allyl alcohol formation on the HTR catalyst is the breaking of the C–D (C–H) bond rather than the addition of hydrogen to acrolein. The increase in the activation energy for H_2–D_2 exchange (from 5 kJ · mol^{-1} for the normal state to 19 kJ · mol^{-1} for the SMSI state) is the reverse of the case of Ir/Nb_2O_5 (*33, 34*).

–CHO is an electron-withdrawing group with $\sigma_m = 0.36$ (σ_m is Hammett's parameter). The influence of the conjugation of C=C and C=O in acrolein can be examined by a comparison with the C=C bond hydrogenation of a nonconjugated molecule having a group with a similar Hammett's parameter instead of a CHO group. We chose CH_2=CH*X* as such a molecule, where *X* is $-CF_3$ ($\sigma_m = 0.43$); $-CF_3$ is expected to be a good reference group because of the stability of the C–F bond and the similarity of σ_m

TABLE 8

HOMO and LUMO Levels of Vinyl Compounds

	Orbital energy (eV)		σ_m
	HOMO	LUMO	
CH_2=$CHNO_2$	−11.63	1.3	0.71
CH_2=$CHCHO$	−10.9	2.6	0.36
CH_2=$CHCF_3$	−11.6	3.6	0.43
CH_2=$CHSiH_3$	−10.4	4.0	
CH_2=CH_2	−10.3	5.1	0
CH_2=$CHCH_3$	−9.9	5.3	−0.07

values. It is well known that Hammett's σ_m is a good reflection of the interaction between the C=C double bond and the transition metal (*37–41*). Pt^0–olefin bond strength has been reported to be determined by the Pt–olefin π-backdonation (*42, 43*); i.e., the higher the LUMO level, the weaker the bond. The HOMO and LUMO levels are summarized in Table 8 (*44*). We can see from the energy levels of vinyl compounds in Table 8 that the electronic state of the C=C bond in CH_2=$CHCF_3$ is a good imitation of that of CH_2=$CHCHO$. Thus we can determine the conjugation effects in hydrogenation of the C=C bond by comparing the reactions of both reactants. In fact, the reaction rates and activation energies for both reactants in Table 1 are not much different, and $\Sigma id_i/n\Sigma d_i$ values, where n is the number of hydrogens involved in hydrogenation/exchange (Tables 3 and 5), are similar for propanal (= 0.42) and 1,1,1-trifluoropropane (= 0.47) and for the LTR catalyst. Interaction of the acrolein C=C bond with Pt is slightly more intense than that for 3,3,3-trifluoropropene, judging from their LUMO energies. In this case, hydrogen, which competes with the unsaturated substrate in adsorption, adsorbs more readily on Pt in the hydrogen/3,3,3-trifluoropropene system than in the hydrogen/acrolein system, resulting in the rapid formation of 1,1,1-trifluoropropane compared with the formation of propanal.

In contrast, C=C hydrogenation on SMSI-Pt/Nb_2O_5 was much slower for 3,3,3-trifluoropropene than for acrolein, as shown in Table 1. The difference between the two reaction rates is 5×10^2, while $\Sigma id_i/n\Sigma d_i$ values are not much different. Considering that the rate-determining step for neither product is hydrogen dissociation on the HTR catalyst, the difference in the kinetic parameters indicates the different reaction intermediates for the hydrogenation of CH_2=$CHCHO$ and CH_2=$CHCF_3$ on the SMSI catalyst. To summarize, the mechanisms for both reactions are suggested to be similar over the LTR catalyst (through the associative adsorption at C=C bond) but different over the HTR catalyst.

(*iii*) *Propanol Formation*

Propanol forms during the initial stage over the LTR catalyst, but is produced only after a certain induction period over the SMSI catalyst. It is clear that allyl alcohol formed during deuteration of acrolein is easily converted to propanol over the LTR catalyst, as shown in Fig. 2. But because of the different behavior of propanol and allyl alcohol (Fig. 3a and the absence of any induction period, all the propanol is not thought to be derived from allyl alcohol.

(*iv*) *Reaction Intermediates*

The most significant difference between LTR and HTR catalysts (Tables 2–4) is the population of deuterium atoms on the terminal carbons of the products. A drastic difference is observed for allyl alcohol (Table 4). γ-Hydrogen in d_1- and d_2-allyl alcohol was selectively deuterium-exchanged on the HTR catalyst, but not on the LTR catalyst, on which α-deuterium and alcoholic deuterium were observed as expected from the usual 1,2-deuterium addition. This feature of deuterium distribution in allyl alcohol was also observed with Ir/Nb_2O_5 (*34*). This suggests the attack of surface deuterium to ter-

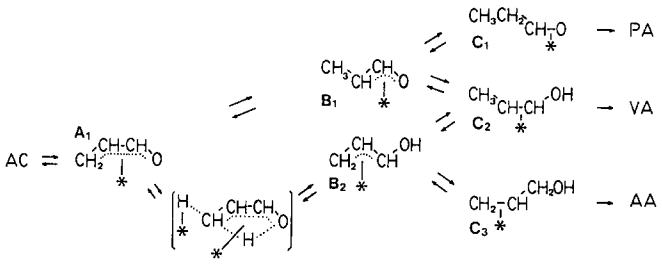

SCHEME 1. Reaction paths and intermediates for acrolein hydrogenation/deuteration on SMSI-Pt/Nb_2O_5. AC, acrolein; PA, propanal; VA, 1-propene-1-ol (vinyl alcohol); AA, 2-propene-1-ol (allyl alcohol).

minal carbon. η^3 (C–C–C)-, η^2 (C–C)- or η^4 (C–C–C–O)-type bonding has been reported for transition metal–acrolein complexes (*45–47*). Several reaction intermediates and schemes including η^2-, η^3-, or η^4-intermediates have been proposed for the hydrogenation of α,β-unsaturated carbonyl compounds (*48–50*). On the basis of these possible intermediates, the previous study on Ir/Nb_2O_5 (*34*) demonstrated that allyl alcohol is produced via a η^4 (C–C–C–O)-intermediate on the HTR catalyst, where surface hydrogen (deuterium) attacks the terminal (γ) carbon of acrolein, resulting in 1,4-hydrogen transfer, as illustrated in Scheme 1.

In addition to the main formation of CHD=$CHCH_2OH$ in d_1-allyl alcohol (Table 4), the large isotope effect in acrolein deuteration (CD_2=CDCDO/CH_2=CHCHO = 10; Table 1), which is attributed to hydrogen abstraction in the rate-determining step, confirms the previous reaction mechanism for allyl alcohol formation involving 1,4-hydrogen transfer in an η^4-intermediate induced by the attack of surface hydrogen atoms on the terminal carbon, as shown in Scheme 1. This is also in agreement with the selective formation of CHD=CHCHO in deuterated acrolein on SMSI catalysts (Table 2). Other possible mechanisms fail to fit the present kinetic data and isotope distributions.

The induction period observed when d_0-acrolein was added during the d_4-acrolein deuteration (Fig. 4c) is attributable to the slow rate of the d_0-acrolein replacement with the preadsorbed d_4-acrolein. Since HD formation under the reaction conditions in Fig. 5 was faster than hydrogenation by a factor of 100, the dissociative adsorption of hydrogen on the HTR catalyst must be fast compared with the addition of deuterium to acrolein-adsorbed species. Therefore, the isotope distribution of allyl alcohol formed after H_2 introduction into the D_2/CD_2=CD-CDO reaction (Fig. 5c) reflects the push–pull reaction from A_1 to B_2 in Scheme 1. Thus, we can estimate the relative probabilities of the hydrogen/deuterium attack on the terminal carbon ($(1-x)/x$) and the 1,4-transfer of hydrogen/deuterium ($(1-y)/y$), which are equivalent to the relative concentrations of hydrogen atoms/deuterium atoms at the metal surface (site I, as discussed below) and those on the terminal carbon of the η^4-intermediate. The relative rates of the steps and the deuterated allyl alcohols produced are shown below:

Step	Relative rate	Product
D-attack and D-transfer	$x \times y \times 0.1$	CD_2=$CDCD_2OD$
H-attack and D-transfer	$(1-x) \times y \times 0.1$	CHD=$CDCD_2OD$
D-attack and H-transfer	$x \times (1-y)$	CD_2=$CDCD_2OH$
H-attack and H-transfer	$(1-x) \times (1-y)$	CHD=$CDCD_2OH$

Note. Normalization factor, $1 - 0.9y$.

The factor 0.1 is taken from the isotope effect in Table 1. The values $x = 0.55$ and $y = 0.8$ give the calculated distribution of the

products, which is in good agreement with the observed distribution as shown in Table 6. The value of $x = 0.55$ implies that surface deuterium is quickly shuffled with hydrogen before reaction with the η^4-intermediate.

The deuterium atom in deuterated propanal formed in the D_2-acrolein reaction was preferentially incorporated into the terminal carbon, as shown in Table 3: $CH_2DCH_2CHO : CH_3CHDCHO = 31 : 4$ and $CHD_2CD_2CHO : CH_3CD_2CHO = 29 : 3$. It is most likely that both allyl alcohol and propanal are formed through the same intermediate on the SMSI catalyst because of the similarity of deuterium incorporation on γ-carbon. The easy conversion of allyl alcohol to propanal (Fig. 2) also indicates a close relation between the mechanisms of formation for both products on the HTR catalyst. On the other hand, allyl alcohol was not transformed to propanal on the LTR catalyst (Fig. 2). The ratio (C–D in γ-carbon)/(C–D in β-carbon) in deuterated propanal on the LTR catalyst is 1.5, showing no selective incorporation of deuterium on γ-carbon. Again, the LTR catalyst showed different isotope distributions in allyl alcohol for both catalysts (Table 4); on the LTR catalyst, deuterium was observed on the C–O position. The hydrogenation of acrolein to form propanal and allyl alcohol on the LTR catalyst can be explained well by the Horiuti–Polanyi mechanism, involving the associative adsorption of C=C and C=O, respectively, followed by hydrogenation (3,4- and 1,2-addition), as shown in Scheme 2. There was no evidence for the coupling of C=O and C=C hydrogenation on the LTR catalyst. The preferable half-hydrogenated species is B_3 rather than B_4 because D on γ-carbon is greater than D on β-carbon.

The rate-determining step of propanal formation on the SMSI catalyst is the addition of hydrogen to B_1 to form C_1. The $A_1 \leftrightarrows B_1$ step is thought to be fast for the following reasons: (1) d_0-allyl alcohol (12%) is formed in the deuteration of d_0-acrolein with D_2, which implies the easy abstraction of methyl hydrogen ($B_1 \rightarrow A_1$) to form surface hydrogen atoms; (2) the step $A_1 \rightarrow B_2$ was found to be the rate-determining step for allyl alcohol formation; and (3) H on the terminal carbon has been observed when the species A_1 is attacked by surface hydrogen/deuterium to form B_2 (Table 6; $(1 - y) = 0.2$). Furthermore, the rate of propanal formation on the HTR catalyst is smaller than that of allyl alcohol, as shown in Table 1. Then the step $B_1 \rightarrow C_1$ must be rate-determining for propanal formation. Vinyl alcohol $CH_3CH{=}CHOH$ is not stable enough to be observed, and it isomerizes to propanal quickly.

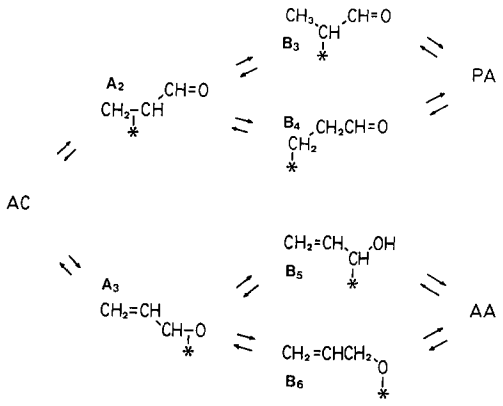

SCHEME 2. Reaction paths and intermediates for acrolein hydrogenation/deuteration on LTR-Pt/Nb_2O_5. AC, acrolein; PA, propanal; AA, 2-propene-1-ol (allyl alcohol).

(v) *Location of the Reaction Site*

Information on the location of active sites can be obtained from the reaction rate as a function of reduction time of catalyst (t_R) (*33, 34*). There are three kinds of surfaces on Pt/Nb_2O_5: the bare Pt metal surface, and the peripheries of the NbO_x and NbO_x islands, which are chemically different. The activities of Nb^{n+} oxides ($n = 3$–5) for hydrogenation under the present conditions were negligible in comparison with those of Pt (*53*). The present attention is, consequently, focused on the bare metal site (site I) and the periphery of NbO_x (site II).

The reaction rate profiles as a function of t_R are similar for the formation of both propanal and allyl alcohol (Fig. 3), suggest-

ing that both reactions proceed on the same type of reaction sites. SMSI generates gradually by increasing the reduction temperature (T_R). At T_R = 623 K, the rate-determining step shifts from the dissociative adsorption of hydrogen to the addition of surface hydrogen to adspecies, as HD formation (Fig. 3) is one order of magnitude higher than propanal and allyl alcohol formation. Thus, the characteristic reaction rate profile at T_R = 623 K in Fig. 3b is suggested to be due to the change in the number of sites (site I and site II) by SMSI generation, similar to the phenomena observed with SMSI-Rh/Nb_2O_5 and Ir/Nb_2O_5 (*33, 34*).

The number of site I and site II changes as a function of t_R is determined by

$$S_I = S_0 - \alpha t_R^{1/2}, \quad S_{II} = \beta t_R^{1/4},$$

where S_0 is the number of site I's on the LTR catalyst without the migration of NbO_x, and α, β are constants. The site I value decreases linearly with $t_R^{1/2}$ because of blocking due to the thermal migration (diffusion) of NbO_x onto the metal surface, while the periphery of NbO_x islands (site II) increases with $t_R^{1/4}$ at the initial stage. The rate of reaction on site I decreases monotonously with t_R, while that on site II initially increases. The reaction rate has a maximum at a certain t_R when site II plays a significant role in catalysis or both sites contribute to the reaction in a coorperative manner (*33, 34*). In the data at T_R = 623 K for HD formation in Fig. 3c, the rate for H_2–D_2 exchange decreased monotonously with an increase in t_R, whereas the rates of formation of propanal and allyl alcohol showed maxima (Fig. 3b). Consequently, hydrogen dissociates on the bare metal site (site I) while acrolein is suggested to adsorb, reacting with hydrogen on the peripheral site (site II). The variation in reaction rates with t_R is similar to that observed in the previous paper on Ir/Nb_2O_5 (*34*). It was, however, reported that on Ir/Nb_2O_5, propanal is formed on site I via an intermediate different from that for allyl alcohol formation, which proceeds on site II.

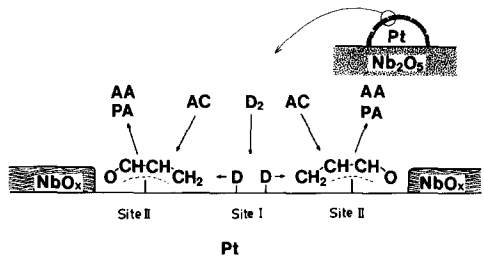

FIG. 6. A schematic model of reaction sites of SMSI-Pt/Nb_2O_5 for acrolein deuteration.

On Pt/Nb_2O_5 both propanal and allyl alcohol are produced on the same site II, as already mentioned; hydrogen atoms are produced on site I as illustrated in Fig. 6.

The value of H/*M* in Fig. 1 decreased from 0.375 to below 0.01 by SMSI, but the rate of H_2–D_2 exchange during acrolein hydrogenation/deuteration decreased only from 1.32 to 0.406 min^{-1}, as shown in Table 1. From these results, the H_2–D_2 exchange reaction per Pt surface metal is considered to be enhanced more than 100 times by SMSI. The above model explains the increase in the rate of H_2–D_2 exchange, which is prevented by the competitive adsorption of acrolein on the LTR catalyst. The model also explains the decrease in $\Sigma id_i/n\Sigma d_i$ in both deuterated propanal and allyl alcohol on the SMSI catalyst. $\Sigma id_i/n\Sigma d_i$ reflects the surface [H]/[D] ratio. Surface deuterium formed by D_2 dissociation is generally diluted by the hydrogen produced by interconversion between the π-intermediate (*A* species in Schemes 1 and 2) and the half-hydrogenated intermediate (*B* species) during deuteration of d_0-acrolein. If the hydrogen atoms diffuse freely on both site I and site II, they would be exchanged with deuterium in the gas phase and as a result the $\Sigma id_i/n\Sigma d_i$ value on the SMSI catalyst would be no different from that on the LTR catalyst having only bare metal sites. The significant difference in $\Sigma id_i/n\Sigma d_i$ values between both catalysts (Tables 3 and 4) implies some restriction of the movement of surface hydrogen into site

II, probably due to the crowdedness of adsorbed acrolein on site II.

Isotope distribution in propanal (Table 7) suggests the identity of chemical environments of active sites for the isomerization of allyl alcohol to propanal and the deuteration of acrolein. If the isomerization and C=C hydrogenation occur on different kinds of sites, d_3-, d_4-, and d_5-propanal should not be produced. This is also consistent with Scheme 1.

(vi) Microscopic Behavior of Active Sites during Reaction

As for the metal–semiconductor junction, the Fermi levels of the metal and the semiconductor must be equal at the interface (*1, 54, 55*). If the work function of TiO_x or NbO_x is smaller than that of the metal, electrons will flow from the suboxides to the metal. Since the screening distance in the metal is usually quite short, it is possible that special electronically modified sites may appear at the interface. Theoretical calculations indicate that the electronic perturbation is screened out within two atomic distances or <0.5 nm (*56–60*). This area may correspond to site II on the SMSI catalyst.

Deuteration of acrolein on SMSI-Pt/Nb_2O_5 occurs by the cooperative work of site I and site II, as illustrated in Fig. 6. Site I dissociates D_2 and site II adsorbs acrolein as A_1 species, which appears to turn its oxygen atom to the NbO_x island. Because deuterium can be supplied only from site I and the isotope distributions in propanal and allyl alcohol show a singular population of D on the γ-carbon. The addition of D atoms to η^4-adsorbate (A_1) produces B_1 and B_2 species, followed by further addition of deuterium or hydrogen to form propanal and allyl alcohol. Singular populations of hydrogen on β-carbon in propanal and α-carbon in allyl alcohol suggest a second addition of H much greater than that of D, which may be due to the spatial restriction of D atom availability. The deuterium population is higher on site I. This difference in "deuterium atmosphere" of reaction sites on SMSI-Pt/Nb_2O_5 has been observed in the D_2-acrolein reaction on Ir/Nb_2O_5 (*34*) and the D_2-ethene reaction on Rh/Nb_2O_5 or Ir/Nb_2O_5 (*33*).

It may be generally expected that SMSI catalysts are favorable for the formation of products requiring less hydrogen. In fact, CO hydrogenation around site II forms higher hydrocarbons more selectively than that on a site I or LTR catalyst (*51, 52*). In acetonitrile hydrogenation on Pt/TiO_2 and Pt/Nb_2O_5, amines are formed in the order secondary > primary > tertiary for the LTR catalyst, but tertiary > secondary > primary (almost zero) for the HTR catalyst (*36*).

The differences in the deuteration mechanism among Pt, Ir, and Rh catalysts are summarized in Table 9. The appearance of two kinds of reaction sites by SMSI is common for the three metals. While Rh was apparently not electronically modified, the other two metals were modified, judging from the difference in activation energies between LTR and HTR catalysts. This might be explained by their Fermi levels. The work functions of the three metals decrease in the order 5.65, 5.27, and 4.98 eV for Pt, Ir, and Rh, respectively. It is difficult to estimate the work function of junctive NbO_x because x and its structure are unknown. Titanium oxide after high-temperature reduction has been reported to have 4.6 eV (*61*) and reduced niobium oxide may be assumed to have a similar value. All of the work functions of Pt, Ir, and Rh are higher than this value, and hence the electrons would flow into the metal. It is possible that acrolein is adsorbed as three kinds of intermediate, η^2(C–C) and η^2(C–O) on site I, and η^4(C–C–C–O) on site II. The former two were observed on both normal Ir/Nb_2O_5 and Pt/Nb_2O_5, and the latter was observed on site II of SMSI-Pt/Nb_2O_5; on SMSI-Ir/Nb_2O_5, however, the three kinds of intermediates were observed. The η^4-type adsorption may be advantageous on electron-rich metal in terms of the delocalization of elec-

TABLE 9

Comparison of Three (Rh, Ir, and Pt) SMSI Catalysts in Ethene and Acrolein Deuteration

Metal (ϕ)	Reaction (E_A)	Adsorption and deuteration	
		Site I	Site II
Rh (4.98 eV)	$CH_2{=}CH_2 + D_2$	D_2 (g) → D (ad) $C_2H_4 \rightarrow \eta^2$ (C–C) (ad)	$C_2H_4 \rightarrow \eta^2$ (C–C) (ad)
	($E_{LTR} = E_{HTR}$)		
		d_2-Ethane, formed	d_0-Ethane, formed
Ir (5.27 eV)	$CH_2{=}CH_2 + D_2$	D_2 (g) → D (ad) $C_2H_4 \rightarrow \eta^2$ (C–C) (ad)	$C_2H_4 \rightarrow \eta^2$ (C–C) (ad)
	($E_{LTR} > E_{HTR}$)		
		d_2-Ethane, formed	d_0-Ethane, formed
	$CH_2{=}CHCH{=}O + D_2$	D_2 (g) → D (ad) AC → η^2 (C–C) (ad) η^2 (C–O) (ad)	AC → η^4 (C–C–C–O) (ad)
	($E_{LTR} < E_{HTR}$; PA) ($E_{LTR} > E_{HTR}$; AA)		
		d_2 – PA + d_2 – AA, formed	d_0 – AA, formed
Pt (5.65 eV)	$CH_2{=}CHCH{=}O + D_2$	D_2 (g) → D (ad)	
			AC → η^4 (C–C–C–O) (ad)
	$E_{LTR} < E_{HTR}$		
		None, formed	d_1, d_2 – AA + d_1, d_2 – PA, formed

Note. E_{LTR} and E_{HTR} represent the activation energies for LTR and HTR catalysts, respectively. AC, PA, and AA are acrolein, propanal, and allyl alcohol, respectively.

trons (indirect interaction). Nb^{n+} ($n < 5$) may also possibly coordinate directly to the oxygen atom of the CHO group of acrolein (direct interaction).

SUMMARY

(1) The structures and microscopic behaviors of reaction sites for acrolein hydrogenation/deuteration on the SMSI-Pt/Nb_2O_5 catalyst were studied by kinetics and isotope distributions.

(2) Selectivity to allyl alcohol formation was enhanced on the HTR catalyst.

(3) Acrolein hydrogenation on the LTR catalyst follows the conventional associative mechanism involving η^2(C–C) or η^2(C–O) species.

(4) In contrast, on the HTR catalyst both propanal and allyl alcohl are formed through η^4-(C–C–C–O)-intermediates.

(5) Hydrogen dissociates on bare metal sites (site I), while acrolein adsorbs to react with hydrogen atoms on the peripheral sites of NbO_x islands (site II) on the HTR catalyst. Accordingly, acrolein hydrogenation proceeds by the cooperative behavior of the two kinds of reaction site on the HTR catalyst.

(6) A comparison with the hydrogenation of $CH_2{=}CHCF_3$ having a CF_3 group with a Hammett's parameter similar to that of the CHO group of acrolein revealed the contribution of the conjugation of C=C and C=O in the acrolein molecule to the adsorption and hydrogenation reaction on the SMSI surface.

(7) The hydrogen-induced γ-C–H breaking mechanism for the hydrogenation of acrolein to allyl alcohol was described in terms of a large isotope effect on the rate and isotope distribution on the γ-carbon of allyl alcohol.

(8) The η^4-(C–C–C–O)-intermediate was

suggested to be stabilized at the conjunction area of metal–NbO_x (site II) by electronic effects.

(9) The D/H ratio of surface concentrations in the D_2/acrolein reaction is lower on site II than on site I.

(10) The reaction rate profiles as a function of reduction time of catalyst, the comparison of HTR and LTR catalysts in the HD formation (H_2 + D_2 + acrolein), the values $\Sigma id_i/n\Sigma d_i$, the reaction rates of acrolein and 3,3,3-trifluoropropene hydrogenations, and the cooperative reaction mechanism discriminate between the two different reaction sites in the working state.

(11) While the value of H/M decreased from 0.375 to below 0.01 by SMSI, site I (bare metal sites) acted as the active site for hydrogen chemisorption and H_2–D_2 exchange reactions, which suggests the heterogeneous distribution of large NbO_x islands on Pt surfaces rather than the uniform and high dispersion of small NbO_x clusters on Pt surfaces.

REFERENCES

1. R. Burch, *in* "Hydrogen Effects in Catalysis" (P. Zoltan and P. G. Menon, Eds.). Dekker, New York, 1988.
2. Tauster, S. J., Fung, S. C., Baker, R. T. K., and Horsley, J. A., *Science* **211,** 1121 (1981).
3. Tauster, S. J., *Acc. Chem. Res.* **20,** 389 (1987).
4. Baker, R. T. K., Tauster, S. J., and Dumesic, J. A., "Strong Metal–Support Interactions," ACS Symposium Series 298. American Chemical Society, Washington, DC, 1986.
5. Imerik, B., Naccache, C., Coudurier, G., Praliaud, H., Meriaudeau, P., Martin, G. A., and Vedrine, J. C., Metal-Additive and Metal–Support Effects in Catalysis. Elsevier, Amsterdam, 1982.
6. Haller, G. L., and Resasco, D. E., *in* "Advances in Catalysis" (D. D. Eley, H. Pines, and P. B. Weisz, Eds.), Vol. 36, p. 173. Academic Press, San Diego, 1989.
7. Resasco, D. E., and Haller, G. L., *J. Catal.* **82,** 279 (1982).
8. Sadeghi, H. R., and Henrich, V. E., *J. Catal.* **87,** 279 (1984).
9. Singh, A. K., Pande, N. K., and Bell, A. T., *J. Catal.* **94,** 422 (1985).
10. Baraunschweig, E. J., Logan, A. D., Datye, A. K., and Smith, D. J., *J. Catal.* **118,** 227 (1989).
11. Meriaudeau, P., Ellestad, O. H., Dufaux, M., and Naccache, C., *J. Catal.* **75,** 243 (1982).
12. Cheu, B., and White, J. M., *J. Phys. Chem.* **86,** 3534 (1982).
13. Burch, R., and Flambard, A. R., *J. Catal.* **78,** 389 (1982).
14. Vannice, M. A., and Garten, R. L., *J. Catal.* **66,** 242 (1980).
15. Kao, C. C., Tsai, S. C., and Chung, Y. W., *J. Catal.* **73,** 136 (1982).
16. Vannice, M. A., and Garten, R. L., *J. Catal.* **56,** 236 (1979).
17. Bartholomew, C. H., Pannell, R. B., and Butler, J. L., *J. Catal.* **65,** 335, (1980).
18. Chung, Y. W., Xiang, G., and Kao, C. C., *J. Catal.* **85,** 237 (1984).
19. Vannice, M. A., and Garten, R. L., *J. Catal.* **63,** 255 (1980).
20. Erdohelyi, A., and Solymosi, F., *J. Catal.* **84,** 446 (1983).
21. Solymosi, F., Tombacz, I., and Erdohelyi, A., *J. Catal.* **75,** 78 (1982).
22. Bracy, J. D., and Burch, R., *J. Catal.* **86,** 384 (1984).
23. Ryndin, Y. A., Hicks, R. F., and Bell, A. T., *J. Catal.* **70,** 287 (1981).
24. Wang, S. J., Moon, S. H., and Vannice, M. A., *J. Catal.* **71,** 167 (1981).
25. Vannice, M. A., and Sudhakar, C., *J. Phys. Chem.* **88,** 2429 (1984).
26. Ko, E. I., Hupp, J. M., and Wagner, N. J., *J. Catal.* **86,** 315 (1984).
27. Kunimori, K., Abe, H., Yamaguchi, E., Matsui, S., and Uchijima, T., *in* "Proceedings, 8th International Congress on Catalysis, Berlin, 1984" Vol. 5, p. 251, Dechema, Frankfurt-au-Main, 1984.
28. Iizuka, T., Tanaka, Y., and Tanabe, K., *J. Mol. Catal.* **17,** 381 (1982).
29. Resasco, D. E., Fenoglio, R. J., Suarez, M. P., and Cechini, J. O., *J. Phys. Chem.* **90,** 4330 (1986).
30. Chou, P., and Vannice, M. A., *J. Catal.* **107,** 129 (1987).
31. Sen, B., and Vannice, M. A., *J. Catal.* **113,** 52 (1988).
32. Vannice, M. A., and Sen, B., *J. Catal.* **115,** 65 (1989).
33. Yoshitake, H., Asakura, K., and Iwasawa, Y., *J. Chem. Soc. Faraday Trans 1,* **84,** 4337 (1988).
34. Yoshitake, H., Asakura, K., and Iwasawa, Y., *J. Chem. Soc. Faraday Trans 1* **85,** 2021 (1989).
35. Takatani, S., and Chung, Y. W., *J. Catal.* **90,** 75 (1984).
36. Yoshitake, H., Asakura, K., and Iwasawa, Y., to be published.
37. Fueno, T., Okuyama, T., Deguchi, T., and Furukawa, T., *J. Amer. Chem. Soc.* **87,** 170 (1965).
38. Fueno, T., Kajimoto, O., and Furukawa, J., *Bull, Chem. Soc. Japan,* **41,** 782 (1968).
39. Yamamoto, T., Nakamura, Y., and Yamamoto, A., *Bull. Chem. Soc. Japan,* **49,** 191 (1976).
40. Tolman, C. A., *J. Amer. Chem. Soc.* **96,** 2780 (1974).

41. Joy, J. R., and Orchin, M., *J. Amer. Chem. Soc.* **81,** 305 (1959).
42. Cenini, S., Ugo, R., and Monica, G. L., *J. Chem. Soc. A,* 409 (1971).
43. Tolman, C. A., Seidel, W. C., and Gerlach, D. H., *J. Amer. Chem. Soc.* **94,** 2670 (1972).
44. Kahn, S. D., Pan, C. F., Overman, L. E., and Hehre, W. J., *J. Amer. Chem. Soc.* **108,** 7381 (1986).
45. Hendrix, W. T., Cowherd, F. G., and Rosenberg, J. L., *J. Chem. Soc. Chem. Commun.,* 98 (1968).
46. Yamamoto, T., Ishizu, J., and Yamamoto, A., *J. Amer. Chem. Soc.* **103,** 6863 (1981).
47. Fritz, H. P., and Schrauzer, G. N., *Chem. Ber.* **94,** 65 (1961).
48. Bond, G. C., "Catalysis by Metals." Academic Press, London, 1962.
49. Touroude, R., *J. Catal.* **65,** 110 (1980).
50. Smith, G. W., and Deany, J. F., *J. Catal.* **6,** 14 (1966).
51. Levin, M. E., Williams, K. J., Salmeron, M., Bell, A. T., and Somorjai, G. A., *Surf. Sci.* **195,** 341 (1988).
52. Levin, M. E., Salmeron, M., Bell, A. T., and Somorjai, G. A., *J. Chem. Soc. Faraday Trans. 1* **83,** 2061 (1988).
53. Nishimura, M., Asakura, K., and Iwasawa, Y., *J. Chem. Soc. Chem. Commun.,* 1660 (1986); *Chem. Lett.,* 573 (1987).
54. Schottky, W., *Z. Phys.* **113,** 367 (1939).
55. Brillson, L. J., *Appl. Surf. Sci.* **11/12,** 249 (1982).
56. Joyner, R. W., Pendry, J. B., Saldin, D. K., and Tennison, S. R., *Surf. Sci.* **95,** 1 (1984).
57. Smith, J. R., Arlinghaus, F. J., and Gay, J. G., *Phys. Rev. B* **26,** 1092 (1982).
58. Feibelman, D. J., and Hamann, D. R., *Surf. Sci.* **149,** 48 (1985).
59. MacLaren, J. M., Pendry, J. B., and Joyner, R. W., *Surf. Sci.* **178,** 856 (1986).
60. MacLaren, J. M., Pendry, J. B., Joyner, R. W., and Meehan, P., *Surf. Sci.* **175,** 263 (1986).
61. Chung, Y. W., Lo, W. J., and Somorjai, G. A., *Surf. Sci.* **64,** 588 (1977).